J Mater Sci (2016) 51:917–925
DOI 10.1007/s10853-015-9420-3

Solvothermal synthesis in ethylene glycol and catalytic activity for CO oxidation of CuO/CeO_2 catalysts

Yu-Ling Zheng[1] · Dong-Sen Mao[1] · Shuai-Shuai Sun[1] · Guang-Ying Fu[1]

Received: 21 July 2015 / Accepted: 7 September 2015 / Published online: 18 September 2015

Abstract A series of supported CuO/CeO_2 catalysts with various CuO loadings (5–25 wt%) were prepared using a solvothermal method with ethylene glycol as solvent. The effects of CuO loading on physicochemical properties and catalytic activity of the prepared CuO/CeO_2 catalysts have been investigated by X-ray diffraction, Raman spectroscopy, BET surface area measurement, X-ray photoelectron spectroscopy, temperature-programmed reduction with H_2, temperature-programmed desorption of CO techniques, and low-temperature CO oxidation reaction test. The results indicate that the catalyst with 10 wt% CuO loading has the highest catalytic activity, which can be attributed to the largest amounts of well-dispersed CuO species strongly interacting with support CeO_2 and oxygen vacancies caused by the incorporation of Cu^{2+} into CeO_2 lattice, and the highest concentration of and the most active lattice oxygen. The activity for CO oxidation of the supported CuO/CeO_2 catalyst prepared by the present solvothermal method was significantly higher than that of the counterparts prepared by the commonly used impregnation and deposition–precipitation methods.

✉ Dong-Sen Mao
dsmao@sit.edu.cn

Yu-Ling Zheng
ylzheng1314@163.com

Shuai-Shuai Sun
126406256@mail.sit.edu.cn

Guang-Ying Fu
fu19900530@sina.com

[1] Research Institute of Applied Catalysis, School of Chemical and Environmental Engineering, Shanghai Institute of Technology, Shanghai 201418, China

Introduction

In recent years, CeO_2 has attracted increasing attention and it was widely applied in environmental catalysis, particularly in the catalytic treatment of automotive exhaust due to its high oxygen storage–release capacity associated with Ce^{4+}/Ce^{3+} redox cycles [1–3]. It was well documented that the catalytic activity of CeO_2 catalyst was greatly promoted not only by precious metals, but also by base metals, particularly copper species [3–8]. The advantages of low price and high catalytic activity in many oxidation reactions, which are comparable to the commercial noble metal catalysts [4–6], make CuO/CeO_2 catalyst strongly competitive. Nowadays, CuO/CeO_2 catalysts are being extensively studied in low-temperature CO oxidation [7–12].

In principle, the formation of Cu–Ce–O solid solution and interaction at $CuO–CeO_2$ junctures can make both components to be reduced and then oxidized more readily. The enhanced catalytic activity in oxidation reactions is believed to be correlated with synergistic redox effect of CuO on CeO_2 and vice versa [13]. The roles of CeO_2 with superior oxygen storage capacity are to promote the dispersion of CuO and to interact with CuO, thus changing their respective physicochemical properties [8, 10, 11]. It is generally recognized that the better dispersion of CuO and the strengthened synergistic effect will be beneficial to the enhancement of catalytic activity toward CO oxidation [8, 10–12].

For CuO/CeO_2 catalysts, different preparation methods have a critical influence on their catalytic activity for CO oxidation [14–18]. Currently, supported CuO/CeO_2 catalysts are usually prepared by impregnation [5, 8, 9, 19] and deposition–precipitation [3, 20] methods. Impregnation method possesses the merit of simplicity and convenience [4], but CuO particles over the CuO/CeO_2 catalysts tend to aggregate, which leads to the poor dispersion of CuO even for low CuO

loadings [9, 20]. The Cu species of samples prepared by deposition–precipitation method are uniformly dispersed, but the preparation process is complex and it is easy for the impurities such as precipitants to get into the catalysts [20]. As a result, various methods have been developed to obtain highly active CuO/CeO_2 catalyst such as template method [21], modified sol–gel method [22], and flame spray pyrolysis [23]. However, these methods generally suffer from some harsh conditions, such as the use of templates [21], and hyperthermal treatment [22, 23]. So it is necessary to explore new simple and effective preparation methods. Compared with the above methods, the solvothermal process has advantages such as simple preparation, inexpensive operation conditions. Besides, the size and shape of the obtained nanoparticles are easily controlled by adjusting reaction time, temperature, and pH in this process [24–26].

In this work, a series of supported CuO/CeO_2 catalysts were prepared via a solvothermal method with ethylene glycol as solvent. The effect of CuO loading on the catalytic performances of the CuO/CeO_2 catalysts for CO oxidation was investigated. For comparison, the catalytic performance of the CuO/CeO_2 catalysts prepared by conventional impregnation and deposition–precipitation methods was also studied. The prepared catalysts were characterized extensively by means of X-ray diffraction (XRD), N_2 adsorption, Raman, XPS, H_2-TPR, and CO-TPD techniques. Furthermore, the catalytic performances of the catalysts were discussed in relation to the results of physicochemical characterization.

Experimental

Preparation of samples

Supported CuO/CeO_2 catalysts with different CuO loadings (5–25 wt%) were prepared by solvothermal method. Commercial CeO_2 support was pretreated at 120 °C for 4 h before use to remove the impurity adsorbed on the surface. After that, support CeO_2 was added to the ethylene glycol solution of $Cu(NO_3)_2{\cdot}3H_2O$ and then reacted at 180 °C for 3 h in a Teflon-lined autoclave with continuous stirring. The suspensions were allowed to cool down to room temperature (RT). The precipitates were separated by filtration, then repeated washing with ethanol, and dried at 120 °C for about 12 h. At last, the samples were calcined in furnace under static air atmosphere at 450 °C for 4 h. The CuO loadings in all the catalysts were expressed as the $CuO/(CuO + CeO_2)$ wt% ratio. The CuO loadings of these catalysts were 5, 10, 15, and 25 wt%, which were denoted as 5-CC, 10-CC, 15-CC, and 25-CC, respectively.

For comparison, on one hand, CuO/CeO_2 catalyst was prepared by impregnating support CeO_2 with an aqueous solution of $Cu(NO_3)_2$ to obtain a CuO loading of 10 wt%. After being impregnated quiescently at RT for 24 h, the sample was dried at 120 °C for 12 h, followed by calcination in static air at 450 °C for 4 h. This catalyst was denoted as 10-CC-IM. On the other hand, CuO/CeO_2 catalyst was prepared by deposition–precipitation method. Briefly, two aqueous solutions of NaOH and $Cu(NO_3)_2$ were simultaneously added to the CeO_2 turbid liquid, and the pH was controlled at approximately 8.0 in the whole precipitation process, then aged in the water bath pot for 3 h at 80 °C. The obtained precipitate was washed with distilled water until pH was decreased to 7.0, followed by washing with ethanol before being dried at 120 °C for about 12 h, and then the dried sample was roasted in static air for 4 h at 450 °C. This catalyst with 10 wt% CuO loading was denoted as 10-CC-DP.

All chemicals used in this work were of reagent grade purity and used as received without further purification (Shanghai Chemical Reagent Corporation, PR China).

Characterization techniques

XRD measurements were conducted with a Rigaku Ultima IV using Cu K_a radiation source generated at 30 kV and 25 mA. Two theta angles ranged from 10° to 90° with a speed of 4° per minute. The crystallite size of CuO was calculated from the XRD spectra by using the Scherrer equation. The cell parameter values were calculated by standard cubic indexation method using the intensity of the CeO_2 (111) peak.

N_2 adsorption–desorption isotherms were obtained at −196 °C on a Micrometrics ASAP- 2020 adsorption apparatus, after all samples (ca. 0.5 g) were degassed under vacuum at 200 °C for 10 h. The specific surface areas were calculated from the linear part of the Brunauer–Emmett–Teller plot.

Raman spectra (at 4 cm^{-1} resolution) were obtained with a DXR-Raman instrument (Thermo Fisher Scientific, American) using the 532 nm exciting line (200 mW beam), 5 scans for each spectrum.

Temperature-programmed reduction with H_2 (H_2-TPR) was carried out by using 10 vol% H_2/N_2 as a reducing gas in a quartz micro-reactor. Approximately, 0.02 g of a freshly calcined catalyst was placed on top of glass wool in the reactor. The outlet of the reactor was connected to a glass column packed with molecular sieve 5 Å in order to remove the moisture produced from reduction. The flow rate of the reducing gas was kept at 50 mL min^{-1}, and the temperature was raised from 50 to 500 °C at a rate of 10 °C min^{-1}. The consumption of H_2 was measured by a thermal conductivity detector (TCD).

The CO adsorption property was measured by temperature-programmed desorption of CO (CO-TPD). The catalyst (0.1 g)

was pretreated under He flow (50 mL min^{-1}) with the temperature ramping from 20 to 500 °C at a rate of 10 °C min^{-1}, and then held at 500 °C for 40 min before being cooled down to RT in He flow. The next step was CO adsorption at RT for 30 min, and then the catalyst was swept again with He for 3 h. Subsequently, the sample was heated in flowing He (50 mL min^{-1}) up to 500 °C at a rate of 10 °C min^{-1}, while the desorbed species was detected with a quadrupole mass spectrometer (QMS, Balzers Omni Star 200).

The surface compositions and chemical states of the samples were investigated by X-ray photoelectron spectroscopy (XPS, kratos Axis Ultra DLD spectrometer), using Al Ká radiation. All the binding energy values were calibrated by using C 1s = 284.6 eV as a reference.

Catalyst activity measurement

The activity measurement was carried out in a fixed bed reactor using 0.2 g of catalyst in 40–60 mesh. The catalyst was loaded between quartz wool plugs in the middle of the reactor. The feed gas consists of 4 vol% CO and 10 vol% O_2 in N_2 at a flow rate of 30 mL min^{-1}. The samples were heated in N_2 (50 mL min^{-1}) at a rate of 10 °C min^{-1} from RT to 200 °C and held at this temperature for 40 min in order to remove possible impurities. After cooling to RT in N_2, the feed gas was introduced into the system. The temperature was increased stepwise (by 5–10 °C), and the catalyst was held for about 30 min at each fixed temperature to achieve steady-state activity. In this case, changes in the catalyst temperature due to heat release because of the possible occurrence of exothermic reactions of CO oxidation were not detected. To allow for the detection of CO and CO_2 with a flame ionization detector (FID), a methanator was inserted between one GC column and the FID. The gas composition after the reaction was analyzed by an on-line gas chromatography with a FID, connected with a computer integrator system. The activity was expressed by the conversion of CO and calculated as follows:

$$\text{CO conversion } (\%) = 100 \times \left([\text{CO}]_{\text{in}} - [\text{CO}]_{\text{out}}\right) / [\text{CO}]_{\text{in}}$$

"In" and "out" as subscripts mean inlet and outlet gaseous stream.

Results and discussion

Characterization of catalysts

XRD study

To clarify the Cu species and crystal phases of the CuO/CeO_2 catalysts with different CuO loadings, the as-prepared samples were identified by XRD. As shown in Fig. 1,

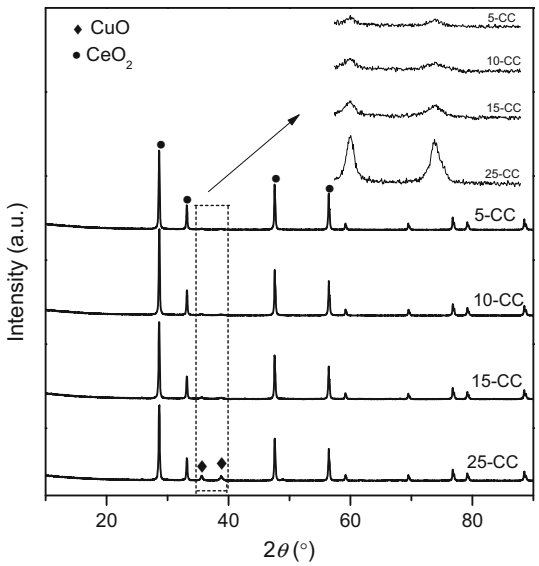

Fig. 1 XRD patterns of CuO/CeO_2 catalysts with different CuO loadings

all the samples exhibit four main reflections at 2θ of 28.8°, 33.3°, 47.9°, and 56.8°, corresponding to the cubic, fluorite structure of CeO_2 phase (JCPDS 34-0394) [27], and the intensity of these peaks remains essentially constant regardless of CuO loading. On the other hand, weak diffraction peaks corresponding to CuO appear at 2θ of 35.5° and 38.7° [JCPDS 41-0254] for all the samples, and the intensity of these peaks increases progressively with the CuO loading increasing from 5 to 25 wt%.

Table 1 shows the crystal sizes of CuO and CeO_2 on the different CuO/CeO_2 catalysts estimated by the Scherrer formula. It can be seen that the crystal size of CuO enlarges with the increase in CuO loading from 5 to 25 wt%, which is connected to excessive Cu species aggregation on the surface of CeO_2. On the other hand, the crystal size of CeO_2 is essentially constant in all of the catalysts, which can be attributed to the commercial CeO_2 support used in these experiments through the high-temperature roasting process.

The lattice parameters obtained from the CeO_2(111) plane are also shown in Table 1. Clearly, lattice constriction has happened on all the CuO/CeO_2 catalysts comparing with support CeO_2, suggesting that some Cu^{2+} ions have been incorporated into the CeO_2 lattice in our catalysts [7, 12].

BET surface area measurement

The BET specific surface areas (S_{BET}) of CeO_2 support and CuO/CeO_2 catalysts are listed in Table 1. It can be seen that the CuO/CeO_2 catalysts exhibit lower S_{BET} compared to CeO_2 support, probably due to the blocking of the pores

Table 1 Structural and textural properties of the CeO_2 support and CuO/CeO_2 catalysts

Sample	D^{a}_{CuO} (nm)	D^{b}_{CeO2} (nm)	S_{BET} (m^2/g)	Lattice parameter[b] (nm)
CeO_2	–	37.9	11.1	0.5414
5-CC	11.3	40.8	7.7	0.5400
10-CC	15.7	40.6	8.1	0.5397
15-CC	19.3	40.0	7.3	0.5400
25-CC	22.2	38.4	6.9	0.5397

[a] The particle size of CuO is the average of the calculated values based on CuO(002) and CuO(111)

[b] The particle size and lattice parameter of CeO_2 are based on CeO_2(111) plane

of CeO_2 by Cu species. On the other hand, all the catalysts show similar BET surface areas (6.9–8.1 $m^2\ g^{-1}$) irrespective of the CuO loading.

Raman analysis

Raman analysis is a potential tool to obtain additional structural information, because it is sensitive to the crystalline symmetry and oxygen lattice vibrations in contrast to the XRD results [28]. Raman spectra of CeO_2 support and different CuO/CeO_2 catalysts are shown in Fig. 2. As shown, all samples exhibit a strong vibration band at about 460 cm^{-1}, corresponding to the F_{2g} Raman vibration mode of fluorite CeO_2 [23]. Clearly, a distinct redshift and a small broadening of the F_{2g} band are observed on all the CuO/CeO_2 catalysts compared with support CeO_2 (466 cm^{-1}). According to the literature [29], the reason of shifting and broadening of the F_{2g} band may be the presence of oxygen vacancies, which is related to structural defects derived from partial incorporation of copper into the ceria lattice, in good agreement with the decrease of lattice parameter microstrain values as shown in Table 1.

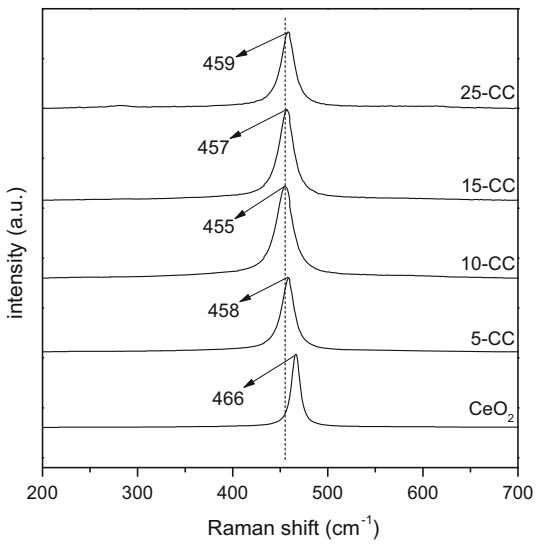

Fig. 2 Raman patterns of CeO_2 support and CuO/CeO_2 catalysts with different CuO loadings

More specifically, as shown in Fig. 2, for the 5-CC and 10-CC catalysts, the peak of the F_{2g} band, respectively, shifts from 466 cm^{-1} for support CeO_2 to 458 and 455 cm^{-1}, and the width of band gradually becomes bigger. However, when the CuO loading is higher than 10 wt%, the peak, respectively, shifts from 455 cm^{-1} for 10-CC to 457 cm^{-1} for 15-CC and 459 cm^{-1} for 25-CC, and the band width decreases slightly. This result suggests that the amount of oxygen vacancies increases first and then decreases with the increase in CuO content, i.e., the 10-CC sample has the largest amount of oxygen vacancies [29].

X-ray photoelectron spectroscopy

In order to illuminate the surface compositions and chemical states of the elements existing in the CuO/CeO_2 catalysts, we further conduct XPS experiments. Table 2 displays the surface atomic compositions of the representative catalysts. It can be seen that the surface Cu/Ce ratios are about 2–4 times higher than the nominal values, which can be expected by the fact that the Cu species mainly deposited on the surface of CeO_2 support. Furthermore, the surface Cu/Ce ratio of the catalyst 15-CC is lower than that of the catalyst 10-CC indicating a poorer dispersion of CuO on the former, which is in good agreement with the formation of larger bulk CuO particles evidenced by the above XRD measurement.

The O 1s, Ce 3d, and Cu $2p_{3/2}$ XPS spectra of the representative CuO/CeO_2 catalysts are shown in Fig. 3a–c. As shown in Fig. 3a, there are two components on the O 1s spectra for all the CuO/CeO_2 catalysts. In addition to the presence of the main peak O′ at 529.5 eV representing the lattice oxygen (O_{lat}) of the metal oxides, an apparent shoulder peak O″ at 531.3 eV attributed to the absorbed oxygen or oxygen in hydroxyl groups is also observed [30]. The percentages of the O_{lat} peak in total O 1s peak for the three catalysts are shown in Table 2. It can be seen that the percentage of O_{lat} peak in the catalyst 10-CC is the largest,

Table 2 XPS data measured for CuO/CeO_2 catalysts with different CuO loadings

Catalyst	Cu/Ce atomic ratio[a]	Ce (III) (%)	O_{lat} (%)[b]	I_{sat}/I^{c}_{pp}	Cu (*I*) (%)[d]
5-CC	0.22(0.11)	13.8	52.4	0.505	39
10-CC	1.02(0.24)	13.8	59.8	0.504	35
15-CC	0.90(0.38)	13.4	49.0	0.504	35

[a] The data in parenthesis are nominal Cu/Ce ratio

[b] The relative intensity of the lattice oxygen to total O 1s peak

[c] The ratio of the intensity of Cu $2p_{3/2}$ satellite peak to that of the principal peak

[d] The ratio of Cu^{+} peak area to the total area in Cu LMM

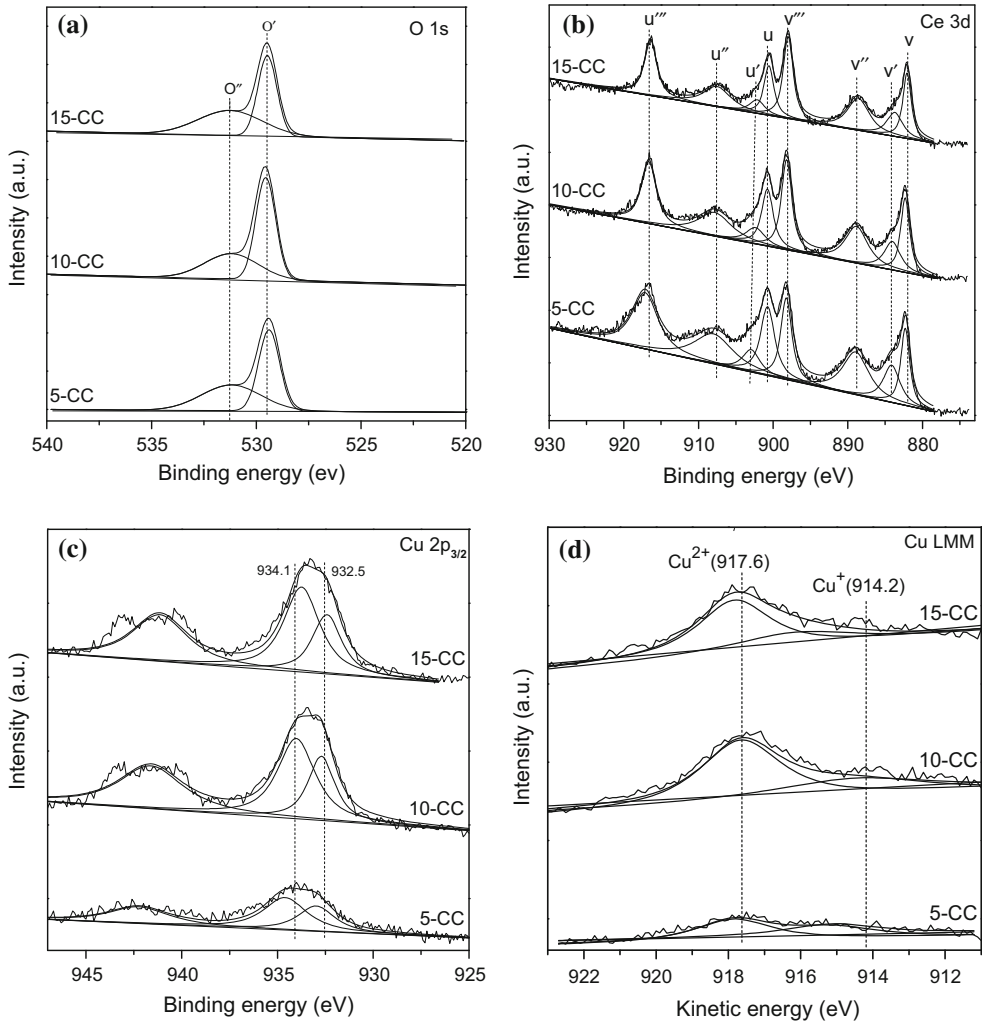

Fig. 3 XPS spectra of CuO/CeO_2 catalysts with different CuO loadings: **a** O 1s, **b** Ce 3d, **c** Cu $2p_{3/2}$, and **d** Cu LMM

indicating that the lattice oxygen amount of the catalyst 10-CC is more than that of the other two catalysts. As mentioned above, oxygen vacancies were created by the substitution of the tetravalent Ce^{4+} cations by divalent Cu^{2+} cations. Oxygen chemisorbed on the catalyst surface can be transformed into lattice oxygen at the oxygen vacancies [31]. This result suggests that the doping of suitable amount of Cu can promote the generation of lattice oxygen.

The Ce 3d XPS data obtained from different CuO/CeO_2 catalysts are shown in Fig. 3b. As illustrated, the peaks marked as u, u″, u‴ and v, v″, v‴ can be ascribed to Ce^{4+}, while those labeled as u′ and v′ can be assigned to Ce^{3+}. Thus, the chemical valence of Ce on the surface of these

catalysts is mainly in a +4 oxidation state, and a small amount of Ce^{3+} co-exists. The amount of Ce^{3+} present on the catalyst surface can be determined by calculating the ratio of area under the peaks of u' and v' to the total area according to the literature [32], and the results are listed in Table 2. We can see that all the catalysts have the similar Ce(III) % values. It should be noted that the values of Ce(III) % for these catalysts are approximately two times higher than that of pure CeO_2 reported in the literature (Ce(III) % = 6.75 %) [33], but the lattice parameters of these samples are similar with the reported one. This phenomenon is probably resulted from the great difference between the two kinds of analytical techniques (XPS and XRD).

By comparing the XPS spectra of Cu $2p_{3/2}$ for different samples (Fig. 3c), Cu^{2+} component (showing the principal peak at about 934.0 eV and the satellite peak at about 942.0 eV) is observed on all the catalysts. Moreover, Cu^{+} or Cu^{0} component (at 932.5 eV) can also be found for these catalysts, which may result from strong interaction of copper species with the CeO_2 support [34, 35], though the reduction of Cu^{2+} under the procedure of XPS measurement cannot be totally ignored [36]. The reduced degree of Cu^{2+} can be investigated by calculating the ratio of the intensities of the satellite peaks to those of the principal peaks (I_{sat}/I_{pp}), which is 0.55 for pure Cu^{2+} [37]. As shown in Table 2, the I_{sat}/I_{pp} values of these CuO/CeO_2 catalysts are similar and lower than 0.55, indicating the appearance of low-valence Cu species in these CuO/CeO_2 catalysts. However, it is less convincing to distinguish between Cu^{+} and Cu^{0} because the Cu $2p_{3/2}$ binding energies and peak shapes of Cu^{+} and Cu^{0} are essentially identical [38].

In order to clarify the low valence state of Cu species, Auger Cu LMM lines were also investigated over these mentioned catalysts. As shown in Fig. 3d, the broad feature of the Cu LMM Auger kinetic energy spectra consists of the contribution of two kinds of Cu species. The peaks at 917.6 and 914.2 eV should, respectively, correspond to the Cu^{2+} and Cu^{+} species as there are no literature data for Cu^{0} with such low Auger kinetic energy [39]. The ratios of Cu^{+} area to the total area (denoted as Cu(I) %), shown in Table 2, for all the catalysts are almost the same, suggesting that the Cu^{+} contents on them are very similar. Note that the Cu(I) % is just calculated for comparison and does not represent the accurate content of Cu^{+} on these CuO/CeO_2 catalysts due to the lower CuO loading and the photoresolution of the spectrometer [40].

H_2-TPR characterization

H_2-TPR experiments were conducted to investigate the reduction properties of the CuO/CeO_2 catalysts. As shown in Fig. 4, there are three peaks (denoted as α, β, and γ, respectively) being detected in all the catalysts. A qualitative attribution of the TPR peaks to different Cu species over CeO_2 support has been proposed by many researchers. For instance, Yen et al. [41] reported two reductive peaks which are attributed to the reduction of well-dispersed surface Cu species and Cu^{2+} in the CeO_2 lattice, respectively. Luo and Avgouropoulos et al. [9, 35] attributed the lower and higher temperature peaks to finely dispersed CuO strongly interacting with CeO_2 and larger CuO particles, respectively. Zou and Moretti et al. [42, 43] suggested, for the more complex H_2-TPR profiles, the contribution of both Cu clusters and isolated Cu^{2+} ions. In this work, based on these literature data and the above XRD results, the α, β, and γ peaks are attributed to reduction of the finely dispersed CuO strongly interacting with CeO_2, Cu species doped into the support CeO_2 lattice, and small two- and three-dimensional clusters of CuO weakly associated with the CeO_2 or larger bulk CuO particles, respectively.

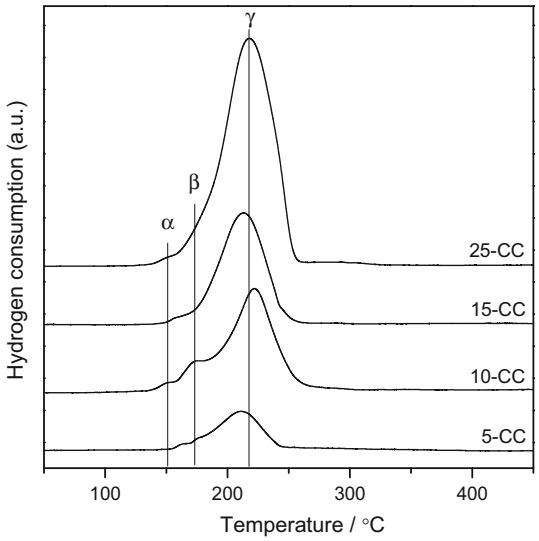

Fig. 4 TPR profiles of CuO/CeO_2 catalysts with different CuO loadings

As shown in Fig. 4, with the increasing of CuO loading from 5 to 10 wt%, the intensity of α and β peaks increases noticeably. However, when the CuO loading is higher than 10 wt%, the intensity of these peaks decreases evidently with the increasing of CuO loading. On the other hand, α peak shifts to a lower temperature first and then shifts toward higher temperatures with the increasing of CuO loading from 5 to 25 wt%. These results suggest that the largest number and the lowest reduction temperature of finely dispersed CuO are achieved on the 10-CC sample. By contrast, the intensity of the γ peak increases gradually with the CuO loading, as a result of CuO particles coalescence and growth, which is in agreement with the above XRD result.

CO-TPD study

TPD profiles of CO_2 after CO adsorption on different CuO/CeO_2 catalysts are presented in Fig. 5. In the heating process, the majority of adsorbed CO desorbs as CO_2 resulting from different carbonates species produced by the reaction of absorbed CO with lattice oxygen [44]. As shown in Fig. 5, there are two CO_2 desorption peaks, i.e., a main peak at lower temperatures and a shoulder peak at higher temperatures. These peaks may be correlated to different CO adsorption approaches: a fraction of CO has formed CO_2 at RT, which probably reacts with CeO_2 surface and adsorbs as carbonate, and then releases at about 100 °C; another fraction of CO probably develops into bidentate carbonate on the reactive sites, which may evolve across intermediate species (maybe as CO_x) when the temperature increases and eventually desorbs as CO_2 at higher temperatures (200–400 °C) [44].

From Fig. 5, all CuO/CeO_2 catalysts exhibit a broad CO_2 desorption peak at 50–250 °C. With the increasing of CuO loading from 5 to 10 wt%, the intensity of CO_2 desorption peaks increases, implying that there are more active lattice oxygen that can interact with the adsorbed CO to form CO_2 at RT, which is beneficial for enhancing the catalytic activity [45]. The enhanced activity of lattice oxygen may result from more finely dispersed CuO and the stronger CuO-CeO_2 synergistic effect. However, at CuO loading higher than 10 wt%, the intensity of CO_2 desorption peaks decreases with the increase in CuO loading. On the other hand, the temperatures of desorption peaks first decrease and then increase with the increase in CuO loading. Evidently, the 10-CC catalyst has the lowest temperature for CO_2 desorption, implying that the produced carbonate species can desorb more easily. These results suggest that the 10-CC catalyst has the largest amount and the most active lattice oxygen among the investigated CuO/CeO_2 catalysts.

Activity measurements

Figure 6 shows the CO oxidation activity patterns of the CuO/CeO_2 catalysts with different CuO loadings. All the catalysts present a similar behavior revealing that the conversion of CO increases with the increase of the catalytic reaction temperature. With the increasing of the CuO loading from 5 to 10 wt%, the activity of the CuO/CeO_2 catalyst is enhanced, but the activity decreases with the further increasing of the CuO loading from 10 to 25 wt%. Clearly, the catalyst with 10 wt% CuO loading exhibits the best catalytic activity. This results indicate that increasing CuO loading can promote the catalytic activity of the CuO/CeO_2 catalysts to some extent, but it is not always so. Liu and Flytzanistephanopoulos [5, 46] suggested that the activity of Cu–Ce–O catalyst derives primarily from the combination of dispersed copper–cerium oxide system, while the bulk CuO particles have negative contribution due to the coverage of active phase species on the catalyst surface. This indicates that the easily reducible and finely dispersed Cu species should be responsible for the activity [47, 48]. Therefore, in our case, the highest activity of the 10-CC catalyst can be reasonably attributed to the largest amount of the well-dispersed Cu species as revealed by the

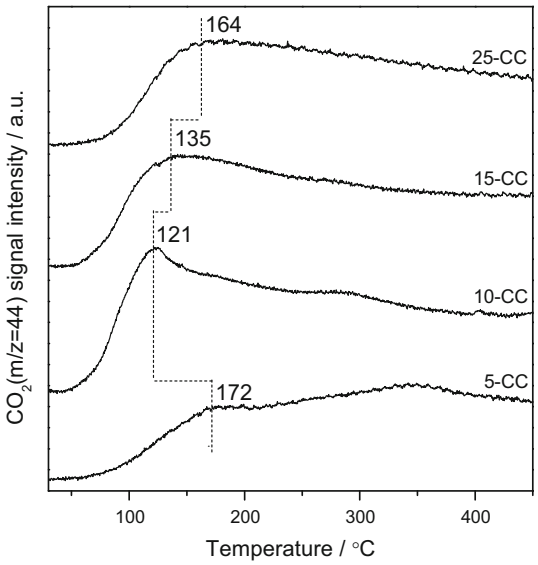

Fig. 5 TPD profiles of CO_2 after CO adsorption at ambient temperature for 30 min over the CuO/CeO_2 catalysts with different CuO loadings

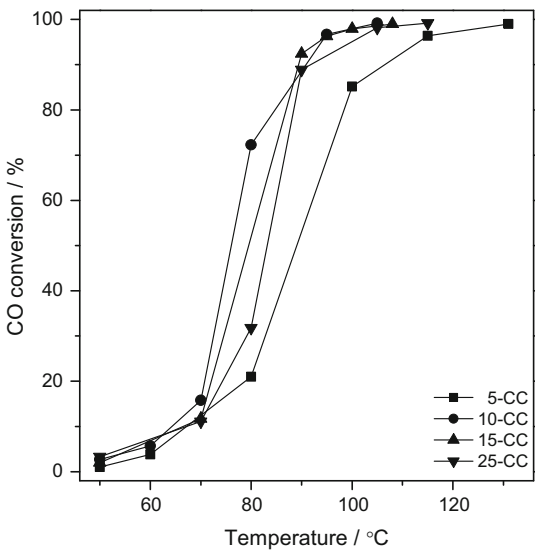

Fig. 6 CO oxidation activities of the CuO/CeO_2 catalysts with different CuO loadings

XRD, surface composition determination, and H_2-TPR results.

On the other hand, it is suggested that the oxidation of CO on CuO/CeO_2 catalyst conforms to the following mechanism [49]: (1) $CO + O_{lat.} \rightarrow CO_2 + O_{vac.}$, (2) $O_2 + 2O_{vac.} \rightarrow 2O_{lat.}$, where the $O_{lat.}$ and $O_{vac.}$ represent lattice oxygen and oxygen vacancy, respectively. Obviously, the larger amounts of lattice oxygen and oxygen vacancy will be favorable to the oxidation of CO. In the case of our catalysts, the 10-CC catalyst possesses the largest amount of and the most active lattice oxygen as revealed by XPS and CO-TPD analyses, respectively, and the largest amount of oxygen vacancy as revealed by Raman analysis, thus exhibiting the highest activity for CO oxidation. Similar results were also reported by other researchers [12, 50].

In order to prove the advantages of the solvothermal method, we have compared the activity of 10-CC prepared by the present solvothermal method with the counterparts prepared by conventional impregnation (10-CC-IM) and deposition–precipitation (10-CC-DP) methods. The CO oxidation activities of the three CuO/CeO_2 catalysts are illustrated in Fig. 7. It can be seen that preparation methods have a significant influence on the catalytic performance of the CuO/CeO_2 catalysts. The catalytic activity of the CuO/CeO_2 catalyst prepared by the solvothermal method is obviously higher than that of the counterparts prepared by the other two methods. T_{100} (i.e., the temperature required for 100 % conversion of CO) for 10-CC, 10-CC-IM, and 10-CC-DP are 105, 145, and 140 °C, respectively. These results indicate that the solvothermal method is a highly effective method for the preparation of CuO/CeO_2 catalyst toward CO oxidation in comparison with the commonly used impregnation and deposition–precipitation methods.

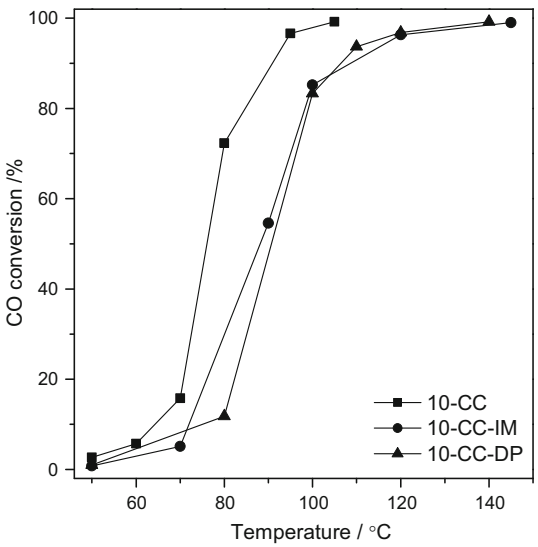

Fig. 7 CO oxidation activities of the CuO/CeO_2 catalysts prepared by different methods

Conclusions

A series of CuO/CeO_2 catalysts with different CuO loadings were synthesized by the simple solvothermal method. The catalyst with 10 wt% CuO (10-CC) shows the highest activity due to the largest amount of well-dispersed CuO. However, excess CuO loadings lead to the CuO aggregation on CeO_2 surface, and the redundant bulk CuO species weaken the catalytic activity. On the other hand, the largest amounts of lattice oxygen and the oxygen vacancies caused by the incorporation of Cu^{2+} into CeO_2 lattice on the 10-CC catalyst are also responsible for the highest activity of the 10-CC catalyst. Moreover, the solvothermal method is a simple and effective method for the preparation of highly active CuO/CeO_2 catalyst for CO oxidation at low temperatures.

Acknowledgements This work was financially supported by the National Natural Science Foundation of China (21273150) and the ''ShuGuang'' Project (10GG23) of Shanghai Municipal Education Commission and Shanghai Education Development Foundation.

References

1. Kang M, Song MW, Lee CH (2003) Catalytic carbon monoxide oxidation over CoO_x/CeO_2 composite catalysts. Appl Catal A 251:143–156
2. Liotta LF, Macaluso A, Longo A et al (2003) Effects of redox treatments on the structural composition of a ceria–zirconia oxide for application in the three-way catalysis. Appl Catal A 240:295–307
3. Tang X, Zhang B, Li Y et al (2005) CuO/CeO_2 catalysts: redox features and catalytic behaviors. Appl Catal A 288:116–125
4. Zimmer P, Tschöpe A, Birringer R (2002) Temperature-programmed reaction spectroscopy of ceria- and Cu/ceria-supported oxide catalyst. J Catal 205:339–345
5. Liu W, Flytzanistephanopoulos M (1995) Total oxidation of carbon monoxide and methane over transition metal fluorite oxide composite catalysts: I. Catalyst composition and activity. J Catal 153:304–316
6. Tschöpe A, Schaadt D, Birringer R et al (1997) Catalytic properties of nanostructured metal oxides synthesized by inert gas condensation. Nanostruct Mater 9:423–432
7. Qi L, Yu Q, Dai Y et al (2012) Influence of cerium precursors on the structure and reducibility of mesoporous $CuO-CeO_2$ catalysts for CO oxidation. Appl Catal B 119–120:308–320
8. Jiang XY, Lu GL, Zhou RX et al (2001) Studies of pore structure, temperature-programmed reduction performance, and microstructure of CuO/CeO_2 catalysts. Appl Surf Sci 173:208–220
9. Luo MF, Zhong YJ, Yuan XX et al (1997) TPR and TPD studies of CuO/CeO_2 catalysts for low temperature CO oxidation. Appl Catal A 162:121–131
10. Liu W, Flytzani-Stephanopoulos M (1996) Transition metal-promoted oxidation catalysis by fluorite oxides: a study of CO oxidation over Cu/CeO_2. Chem Eng J 64:283–294

11. Sedmak G, Hočevar S, Levec J (2004) Transient kinetic model of CO oxidation over a nanostructured $Cu_{0.1}Ce_{0.9}O_{2-y}$ catalyst. J Catal 222:87–99
12. Jia AP, Hu GS, Meng L et al (2012) CO oxidation over CuO/$Ce_{1-x}Cu_xO_{2-\delta}$ and $Ce_{1-x}Cu_xO_{2-\delta}$ catalysts: synergetic effects and kinetic study. J Catal 289:199–209
13. Dow WP, Wang YP, Huang TJ (2000) TPR and XRD studies of yttria-doped ceria/γ-alumina-supported copper oxide catalyst. Appl Catal A 190:25–34
14. Avgouropoulos G, Ioannides T, Matralis H (2005) Influence of the preparation method on the performance of CuO–CeO_2 catalysts for the selective oxidation of CO. Appl Catal B 56:87–93
15. Gamarra D, Munuera G, Hungría AB et al (2007) Structure − activity relationship in nanostructured copper − ceria-based preferential CO oxidation catalysts. J Phys Chem C 111:11026–11038
16. Sirichaiprasert K, Luengnaruemitchai A, Pongstabodee S (2007) Selective oxidation of CO over Cu–Ce–Fe–O composite oxide catalyst in hydrogen feed stream. Int J Hydrog Energy 32:915–926
17. Liu Z, Zhou R, Zheng X (2008) Influence of preparation methods on CuO-CeO_2 catalysts in the preferential oxidation of CO in excess hydrogen. J Nat Gas Chem 17:125–129
18. Liu Z, Yang S, Zhou R et al (2010) Influence of pH values in the preparation of CuO-CeO_2 on its catalytic performance for the preferential oxidation of CO in excess hydrogen. J Nat Gas Chem 19:313–317
19. Zheng XC, Wu SH, Wang SP et al (2005) The preparation and catalytic behavior of copper–cerium oxide catalysts for low-temperature carbon monoxide oxidation. Appl Catal A 283:217–223
20. Tang X, Zhang B, Li Y et al (2004) Carbon monoxide oxidation over CuO/CeO_2 catalysts. Catal Today 93–95:191–198
21. Zhu J, Gao Q, Chen Z (2008) Preparation of mesoporous copper cerium bimetal oxides with high performance for catalytic oxidation of carbon monoxide. Appl Catal B 81:236–243
22. Luo MF, Song YP, Lu JQ et al (2007) Identification of CuO species in high surface area CuO − CeO_2 catalysts and their catalytic activities for CO oxidation. J Phys Chem C 111:12686–12692
23. Kydd R, Teoh WY, Wong K et al (2009) Flame-synthesized ceria-supported copper dimers for preferential oxidation of CO. Adv Funct Mater 19:369–377
24. Pimentel A, Rodrigues J, Duarte P et al (2015) Effect of solvents on ZnO nanostructures synthesized by solvothermal method assisted by microwave radiation: a photocatalytic study. J Mater Sci 50:5777–5787. doi:10.1007/s10853-015-9125-7
25. Zeng SH, Liu KW, Chen TJ et al (2013) Influence of crystallite size and interface on the catalytic performance over the CeO_2/CuO catalysts. Int J Hydrog Energy 38:14542–14549
26. Mrabet D, Abassi A, Cherizol R et al (2012) One-pot solvothermal synthesis of mixed Cu-Ce-Ox nanocatalysts and their catalytic activity for low temperature CO oxidation. Appl Catal A 447–448:60–66
27. Cao JL, Wang Y, Zhang TY et al (2008) Preparation, characterization and catalytic behavior of nanostructured mesoporous CuO/$Ce_{0.8}Zr_{0.2}O_2$ catalysts for low-temperature CO oxidation. Appl Catal B 78:120–128
28. Fernández-García M, Martínez-Arias A, Iglesias-Juez A et al (2000) Structural characteristics and redox behavior of CeO_2-ZrO_2/Al_2O_3 supports. J Catal 194:385–392
29. Gnanakumar ES, Naik JM, Manikandan M et al (2014) Role of nanointerfaces in Cu- and Cu + Au- based near-ambient-temperature CO oxidation catalysts. ChemCatChem 6:3116–3124
30. Li J, Zhu P, Zuo S et al (2010) Influence of Mn doping on the performance of CuO-CeO_2 catalysts for selective oxidation of CO in hydrogen-rich streams. Appl Catal A 381:261–266
31. Zou H, Chen S, Liu Z et al (2011) Selective CO oxidation over CuO-CeO_2 catalysts doped with transition metal oxides. Powder Technol 207:238–244
32. Reddy LH, Reddy GK, Devaiah D et al (2012) A rapid microwave-assisted solution combustion synthesis of CuO promoted CeO_2-M_xO_y (M = Zr, La, Pr and Sm) catalysts for CO oxidation. Appl Catal A 445–446:297–305
33. Cai W, Chen F, Shen X et al (2010) Enhanced catalytic degradation of AO7 in the CeO_2–H_2O_2 system with Fe^{3+} doping. Appl Catal B 101:160–168
34. Cao JL, Shao GS, Ma TY et al (2009) Hierarchical meso–macroporous titania-supported CuO nanocatalysts: preparation, characterization and catalytic CO oxidation. J Mater Sci 44:6717–6726. doi:10.1007/s10853-009-3583-8
35. Kundakovic L, Flytzani-Stephanopoulos M (1998) Reduction characteristics of copper oxide in cerium and zirconium oxide systems. Appl Catal A 171:13–29
36. Zhu H, Shen M, Kong Y et al (2004) Characterization of copper oxide supported on ceria-modified anatase. J Mol Catal A 219:155–164
37. Avgouropoulos G, Ioannides T (2006) Effect of synthesis parameters on catalytic properties of CuO-CeO_2. Appl Catal B 67:1–11
38. Wang SP, Zheng XC, Wang XY et al (2005) Comparison of CuO/$Ce_{0.8}Zr_{0.2}O_2$ and CuO/CeO_2 catalysts for low-temperature CO oxidation. Catal Lett 105:163–168
39. He C, Yu Y, Yue L et al (2014) Low-temperature removal of toluene and propanal over highly active mesoporous $CuCeO_x$ catalysts synthesized via a simple self-precipitation protocol. Appl Catal B 147:156–166
40. Sun SS, Mao DS, Yu J et al (2015) Low-temperature CO oxidation on CuO/CeO_2 catalysts: the significant effect of copper precursor and calcination temperature. Catal Sci Technol 5:3166–3181
41. Yen H, Seo Y, Kaliaguine S et al (2012) Tailored mesostructured copper/ceria catalysts with enhanced performance for preferential oxidation of CO at low temperature. Angew Chem Int Ed 51:12032–12035
42. Zou H, Dong X, Lin W (2006) Selective CO oxidation in hydrogen-rich gas over CuO/CeO_2 catalysts. Appl Surf Sci 253:2893–2898
43. Moretti E, Storaro L, Talon A et al (2011) Effect of thermal treatments on the catalytic behaviour in the CO preferential oxidation of a CuO–CeO_2–ZrO_2 catalyst with a flower-like morphology. Appl Catal B 102:627–637
44. Caputo T, Lisi L, Pirone R et al (2008) On the role of redox properties of CuO/CeO_2 catalysts in the preferential oxidation of CO in H_2-rich gases. Appl Catal A 348:42–53
45. Martínez-Arias A, Fernández-García M, Gálvez O et al (2000) Comparative study on redox properties and catalytic behavior for CO oxidation of CuO/CeO_2 and CuO/$ZrCeO_4$ catalysts. J Catal 195:207–216
46. Liu W, Flytzanistephanopoulos M (1995) Total oxidation of carbon monoxide and methane over transition metal fluorite oxide composite catalysts: II. Catalyst characterization and reaction kinetics. J Catal 153:317–332
47. Cao JL, Deng QF, Yuan ZY (2009) Mesoporous $Ce_{0.8}Zr_{0.2}O_2$ solid solutions-supported CuO nanocatalysts for CO oxidation: a comparative study of preparation methods. J Mater Sci 44:6663–6669. doi:10.1007/s10853-009-3582-9
48. Fu GY, Mao DS, Sun SS et al (2015) Preparation, characterization and CO oxidation activity of Cu-Ce-Zr mixed oxide catalysts via facile dry oxalate-precursor synthesis. J Ind Eng Chem 31:283–290
49. Liu Y, Wen C, Guo Y et al (2010) Modulated CO oxidation activity of M-doped ceria (M = Cu, Ti, Zr, and Tb): role of the pauling electronegativity of M. J Phys Chem C 114:9889–9897
50. Li J, Han Y, Zhu Y et al (2011) Purification of hydrogen from carbon monoxide for fuel cell application over modified mesoporous CuO–CeO_2 catalysts. Appl Catal B 108–109:72–80